STIF

NASA Technical Memorandum 89463

Transport of Passive Scalars in Turbulent Channel Flow

John Kim and Parviz Moin

July 1987

National Aeronautics and
Space Administration

NASA Technical Memorandum 89463

Transport of Passive Scalars in Turbulent Channel Flow

John Kim,
Parviz Moin, Ames Research Center, Moffett Field, California

July 1987

National Aeronautics and
Space Administration

Ames Research Center
Moffett Field, California 94035

TRANSPORT OF PASSIVE SCALARS IN A TURBULENT CHANNEL FLOW

John Kim and Parviz Moin

NASA Ames Research Center, Moffett Field, California 94035

ABSTRACT

A direct numerical simulation of a turbulent channel flow with three passive scalars at different molecular Prandtl numbers is performed. Computed statistics including the turbulent Prandtl numbers are compared with existing experimental data. The computed fields are also examined to investigate the spatial structure of the scalar fields. The scalar fields are highly correlated with the streamwise velocity; the correlation coefficient between the temperature and the streamwise velocity is as high as 0.95 in the wall region. The joint probability distributions between the temperature and velocity fluctuations are also examined; they suggest that it might be possible to model the scalar fluxes in the wall region in a manner similar to the Reynolds stresses.

INTRODUCTION

The transport of heat and contaminants in turbulent flows is of great importance in many engineering applications. Heat-transfer problems in heat exchangers, gas turbines, and nuclear reactors, and pollution dispersal in urban atmospheres are a few examples. In general, a turbulent flow field causes fluctuations in a scalar field through turbulent convection whereas the fluctuating scalar field influences the velocity field through mean gradients and density changes. For small temperature differences or small concentration of contaminants, however, the turbulent velocity field drives the scalar field, and the influence of the latter on the former is rather weak and can be neglected. In these cases, a passive scalar field can be determined independently by solving the conservation equation of the passive scalar for a given turbulent velocity field.

In solving the Reynolds-averaged conservation equation for a passive scalar, one encounters the same turbulence closure problem as in solving the governing equations for the velocity field. In the simplest approach, one uses the effective eddy conductivity (or diffusivity) to relate the scalar fluxes to mean flow variables in analogy to the eddy viscosity in the momentum transport. Since the turbulent velocity field is assumed to be known, the eddy viscosity is known, and a knowledge of the turbulent Prandtl number (or Schmidt number for mass transfer), defined as a ratio of the eddy viscosity to the eddy conductivity (diffusivity), is sufficient to solve the conservation equation for the scalar field. A large number of experimental works on the turbulent Prandtl number for various fluids can be

Presented at the Sixth Symposium on Turbulent Sheet Flows,
Toulouse, France; September 7-9, 1987

found in the literature: see, Eckelman and Hanratty (1972), McEligot et al. (1976), Antonia (1980), Malhotra & Kang (1984), to name a few. Reynolds (1975) provides a survey on more than 30 models for predicting the turbulent Prandtl number.

In the second-moment closure approach, one dispenses with the eddy-diffusivity model and directly solves the Reynolds-averaged transport equations for the scalar fluxes. This approach is equivalent to solving the transport equations for the Reynolds stresses in the momentum transport. In the second-moment closure, the transport equations for the scalar fluxes contain many terms that have to be modeled. But a justification for this approach is that approximations are made at more fundamental levels, and, hence, they will be applicable for more general situations. To some extent, this justification has been validated in the modeling of the momentum transport, and it is likely that this will hold for the transport of passive scalars. Interested readers should refer to Lumley & Khajeh-Nouri (1974) and Launder (1978) for further details.

In this paper we study numerically the turbulent transport of passive scalars in a channel flow by directly solving the unsteady, three-dimensional Navier-Stokes equations and the equations for passive scalar fields simultaneously. The resulting solutions contain detailed information on the velocity and the passive scalar fields. Time-averaged statistics, as well as turbulence structures associated with the velocity field, are reported in detail by Kim et al. (1987). The objective of the present paper is to present results pertaining to the transport of passive scalars in turbulent flows. Other details such as budgets for the scalar fluxes, essential information for developing the second-moment closure models, will be reported elsewhere.

Throughout the present paper, we use temperature as our passive scalar (heat transfer), but this can be replaced with a mass concentration (mass transfer). Likewise, for example, thermal diffusivity, heat flux, and Prandtl number can be replaced with, respectively, concentration diffusivity, mass flux, and Schmidt number.

In the first part of the paper, turbulence statistics including the turbulent Prandtl number associated with fully developed scalar fields for three different molecular Prandtl numbers (0.1, 0.71 and 2) are presented. In the second part of the paper, we examine the correlations between the velocity and scalar fields. Air ($Pr = 0.71$) was chosen as the medium for this purpose. The wall-layer structures identified by the temperature field are compared with the structures found in the velocity field. The role of the organized turbulence structures in scalar transport is discussed.

NUMERICAL PROCEDURES

The unsteady Navier-Stokes equations were solved numerically at a Reynolds number of 3300, based on the mean centerline velocity and the channel half-width (180 based on the wall shear velocity and the channel half-width), with about 2×10^6 grid points ($128 \times 129 \times 128$ in x, y, and z). A spectral method — Fourier series in the streamwise and spanwise directions and Chebyshev polynomial expansion in the normal direction — was used for spatial derivatives. The time advancement was made by a semi-implicit method:

the Crank-Nicolson scheme for viscous terms and the Adams-Bashforth method for the nonlinear terms. Further information on the numerical method can be found in Kim et al. (1987). No subgrid-scale model was used in the computation since the grid resolution was sufficiently fine to resolve all the essential turbulent scales. Grotzbach (1981) performed similar numerical simulations with subgrid scale models for high Reynolds number flows.

Once the velocity field was advanced for each time step, the corresponding scalar fields were obtained by integrating the following conservation equations for scalars:

$$\frac{\partial \theta_i}{\partial t} + \frac{\partial}{\partial x_j}\theta_i u_j = \frac{1}{Re\, Pr_i}\frac{\partial^2 \theta_i}{\partial x_j \partial x_j} + Q_i \quad \text{(no summation over } i\text{)} \tag{1}$$

where the θ_i $(i = 1,2,3)$ represent three different scalars, Re and Pr_i denote the Reynolds number and the molecular Prandtl numbers, and Q_i represents a source term for each scalar field. All the variables are nondimensionalized by the wall shear velocity, u_τ, channel half-width, δ, and a reference temperature, θ_r. With these nondimensionalizations, the Reynolds number and the Prandtl number are defined as $Re = u_\tau \delta/\nu$ and $Pr_i = \nu/\alpha_i$, where ν and α_i are kinematic viscosity and thermal diffusivity, respectively.

The initial field for the velocity was taken from the simulation of Kim et al. (1987). This represents a fully developed turbulent channel flow. Two different initial and boundary conditions were used for the scalar fields. In case I, the initial and boundary conditions were given as follows:

$$\begin{aligned} &\theta_i(x,y,z,0) = 0.5(1-y^2) \\ &\theta_i(x,-1,z,t) = 0, \quad \theta_i(x,1,z,t) = 0 \end{aligned} \tag{2}$$

with $Q_i = 2/(Re\, Pr_i)$. This represents a case in which the passive scalar is created internally and removed from both walls. In case II, the initial and boundary conditions were given as follows:

$$\begin{aligned} &\theta_i(x,y,z,0) = erfc\left(\frac{1+y}{2\sqrt{Re\, Pr_i\, y_0}}\right) \\ &\theta_i(x,-1,z,t) = 1, \quad \theta_i(x,1,z,t) = 0 \end{aligned} \tag{3}$$

where $erfc$ denotes the complementary error function, and y_0 is an arbitrary constant which determines the initial thickness of the thermal boundary layer at the lower wall. The source terms were turned off (Q_i=0) for case II. This represents a case in which the passive scalars were introduced at the lower wall ($y = -1$), and removed from the upper wall ($y = 1$). In the present paper, all the results are from case I, unless otherwise specified. Details of the results obtained from case II will be reported elsewhere.

STATISTICS OF PASSIVE SCALARS

The computations were carried out until the passive scalar fields reached statistically steady states. The initial velocity field was taken from a previous calculation in which the velocity field already had reached a statistically steady state.

Profiles of the mean and rms fluctuations of the scalar fields from case I are shown in Fig. 1. Since all the statistical quantities to be presented in this paper are symmetric about the centerline of the channel, only the statistics from one side of the channel are shown; it is implied that y is measured from that wall, although in some cases, y_w is used explicitly to avoid confusion. The passive scalars are nondimensionalized by the wall surface scalar flux defined as

$$\theta_\tau = \frac{\dot{q}_w}{\rho c_p u_\tau} = \frac{k \frac{\partial \theta}{\partial y}\Big|_w}{\rho c_p u_\tau} = \frac{\alpha \frac{\partial \theta}{\partial y}\Big|_w}{u_\tau}$$

where ρ and c_p are the fluid density and the specific heat at constant pressure, respectively, and $\alpha = k/(\rho c_p)$. The surface heat flux θ_τ is sometimes referred to as the friction temperature in analogy to the friction velocity, u_τ. Throughout the paper the superscript $+$ indicates a nondimensional quantity scaled by the wall variables; for example, $y^+ = y u_\tau/\nu$ and $\theta_i^+ = \theta_i/\theta_{\tau_i}$.

In Fig. 1a, where the mean scalar profiles are shown in semilogarithmic coordinates, the formulas recommended by Kader (1981) are also included. Kader suggested this formula, which is a function of the molecular Prandtl number, as well as Reynolds number, for the mean temperature profile after examining several experimental results. As shown in the figure, the agreement between the computed results and Kader's formula is remarkable. This is especially so since all the experimental data Kader considered were at much higher Reynolds numbers than the present one.

The rms fluctuations for each scalar field are shown in Fig. 1b, together with the experimental data from a slightly heated turbulent boundary layer obtained by Subramanian and Antonia (1981). The experimental data shown correspond to $Pr = 0.71$ and their lowest Reynolds number ($Re_m = 990$ based on the momentum thickness and the channel half-width, compared to 280 for the present case). With the wall scaling, it is expected that the two results should agree in the wall region, and indeed the agreement is quite good. The locations of peak rms value move away from the wall as the molecular Prandtl number decreases. The thickness of thermal boundary layers defined as

$$\Delta_T = \int_0^1 \frac{\overline{\theta}_{c_i} - \overline{\theta}_i}{\theta_{\tau_i}} \, dy$$

was 1.6, 2.4, and 2.8, for $Pr = 0.1$, 0.71, and 2, respectively, where $\overline{\theta}_{c_i}$ is the mean temperature at the centerline. The corresponding Clauser thickness — a similar measure of the momentum layer — was 2.7. The variation in the thermal boundary-layer thicknesses indicates the breakdown of the "Reynolds analogy."

The normal heat fluxes, $\overline{\theta' v'}$, and their correlation coefficients are shown in Fig. 2. With the present normalization, the normal heat flux represents a ratio of the normal heat flux

to the surface heat flux ($\overline{\theta' v'}/\dot{q}_w$). Again the symbols represent the data from Subramanian and Antonia. Note that, for the fully developed channel flow, $-\overline{\theta' v'} + (1/RePr)\bar{\theta}_{,y} = 1 - y_w$ when a steady state is reached, and the data are indeed very close to the straight line. The agreement with the experimental data is poor, but this is probably a result of the difference in Reynolds numbers and the difference between the two flows (channel vs boundary layer). For example, the correlation coefficient for the present case must be zero at the channel centerline, whereas the experimental data from the boundary layer can remain finite at the edge of the boundary layer. Figure 2b indicates that the correlation coefficient decreases with an increase in the molecular Prandtl number.

Figure 3 shows the axial heat fluxes and their correlation coefficients. Again, the axial heat flux normalized in the present form represents a ratio of the axial heat flux to the surface heat flux. Unlike the normal heat fluxes, which should be < 1, the axial heat fluxes are > 1 for most regions except the lowest Prandtl number case. The agreement between the computed results and the experimental results is good away from the wall, but poor near the wall. The correlation coefficients between the temperature and the axial velocity are also much higher than those between the temperature and the normal velocity. In the wall region, the correlation coefficients are as large as 0.95 for the two high-Prandtl-number cases. It is also interesting to note that in the wall region, the correlation coefficients of $\overline{\theta' u'}$ for the higher molecular Prandtl number cases are larger than that for the lowest Prandtl number case, which is different from the trend of the correlation coefficients of $\overline{\theta' v'}$. The agreement with the experimental data is satisfactory except near the centerline of the channel, where agreement is not expected.

Profiles of eddy viscosity, diffusivity, and turbulent Prandtl number are shown in Fig. 4. The low-Prandtl-number case is quite different from the other two, whereas there exists almost no difference between the cases of $Pr = 0.71$ and 2. The turbulent Prandtl number for the case of $Pr = 0.1$ remains > 1, and that for the case of $Pr = 0.71$ and 2 has a maximum value of about 1.1 at the wall and decreases slightly away from the wall and remains at values < 1. From experimental observations, it is generally accepted that $Pr_T < 1$ for $Pr > 1$, and $Pr_T > 1$ for $Pr < 1$ (Reynolds, 1975), which is consistent with the present results. For all three cases, the turbulent Prandtl numbers have local maximums at $y/\delta \approx 0.25$ ($y^+ \approx 45$). It is interesting to note that the turbulent Prandtl numbers approach the same constant value (about 1.1) as the wall is approached, independent of the molecular Prandtl numbers. The same behavior was also observed for case II (not shown here). Deissler (1963) showed in his analysis of homogeneous turbulence with a uniform velocity gradient that the turbulent Prandtl number approached one at high velocity gradients independent of the molecular Prandtl number.

STRUCTURE OF THE SCALAR FIELDS

For case II, the time evolution of the scalar fields corresponding to temperature of air ($Pr = 0.71$) was also examined, since this made it possible to trace the turbulence structures originating from the wall region. Figure 5 shows contour plots of temperature

in an (x,y)-plane. The contours clearly show the existence of large-scale structures that bulge out from the wall region. Note that there exist sharp temperature gradients along the upstream edge of the large-scale structures. This structure was referred to as the temperature front by Chen & Blackwelder (1978) in their study of turbulence structures in a turbulent boundary layer.

Contours of u', θ', and $\theta'v'$ in the (x,z)-plane at $y^+ \approx 5$ are shown in Fig. 6. Contours of streamwise velocity fluctuations (Fig. 6a) display the well-known wall-layer streaky structures. Their mean spanwise spacing is about 100 in wall units. The contours of temperature fluctuations shown in Fig. 6b show nearly identical streaky structures. The regions of low and high temperature are elongated in the streamwise direction with a mean spanwise spacing of about 100 in wall units — the mean spanwise spacings were determined by examining the two-point correlations of the temperature fluctuations in the spanwise direction as in the case of the low-speed streaks (see Kim et al. 1987). It is clear from Fig. 6a and 6b that the temperature in the near-wall region is highly correlated with the streamwise velocity; the low-speed fluid is associated with low-temperature regions and the high-speed fluid with high temperature. In fact, the correlation coefficient at this y-location is about 0.95 (Fig. 3). Figures 6a and 6b are consistent with the experimental observation of Iritani et al. (1983), who performed simultaneous visualizations of velocity and temperature fields in a turbulent boundary layer, using hydrogen bubbles for the velocity field and surface-mounted, liquid-crystal sheets sensitive to the wall temperature for the scalar field. Figure 6c shows the contours of $\theta'v'$; they display intermittent regions of large $\theta'v'$ similar to the spatial distribution of $u'v'$. This implies that production of the scalar fluctuations $(-\overline{\theta'v'}\partial\overline{\theta}/\partial y)$ also takes place intermittently just as that of the velocity fluctuations. In fact, contour plots of corresponding $u'v'$ (not shown) are almost identical to those in Fig. 6c.

Contours of the surface heat flux are shown in Fig. 7. By comparing this figure with Fig. 6a we find that the regions of high surface-heat flux coincide with the regions of high-speed fluid. Regions covered by the low-speed streaks do not have high heat transfer at the wall. The rms fluctuation of the surface heat flux is 0.38 $\dot{q}_w$. The maximum surface heat flux in Fig. 7 is about 3 times the mean surface heat flux, and the minimum was about 40 % of the mean value, indicating that the distribution of the surface heat flux fluctuation is positively skewed.

The high correlations between the streamwise velocity and temperature can be also seen in Fig. 8, where the joint probability distributions of (u',v'), (u',θ'), and (θ',v') at $y^+ \approx 5$ are shown. Note that a straight line would indicate a perfect correlation, and Fig. 8 indicates a strong positive correlation between u' and θ', and a mild negative correlations between θ' and v'. Because of the high correlation between u' and θ', the joint probability distribution of θ' and v' (Fig. 8b) is very similar to that of u' and v' (Fig. 8c). Examination of higher-order statistical correlations, such as skewness and flatness factors, also indicate a strong similarity between u' and θ' in the wall region. This strong similarity in the behavior of the streamwise velocity and temperature can be observed also in the two-point correlations of the streamwise velocity and temperature fluctuations as shown in Fig. 9. At

this y-location, there exists practically no difference between R_{uu} and $R_{\theta_i\theta_i}$, even though the highest Prandtl number is 20 times the lowest one. The streaky structures of the streamwise velocity fluctuations, which can be identified with the long correlation length in the streamwise direction (order of $\Delta x^+ \approx 1000$) and the negative peaks in the spanwise correlation (at about $\Delta z^+ \approx 50$), are so dominant in the wall region it appears that these structures are imposed onto the scalar fields almost independent of the molecular Prandtl number. This is rather surprising since the sublayer of the thermal boundary layer is a strong function of the Prandtl number (Fig. 1a). Obviously this Prandtl-number independence cannot be true in the limit $Pr \rightarrow 0$, and this is reflected somewhat in the two-point correlations for $Pr = 0.1$. This situation changes significantly away from the wall, where the two-point correlations of the temperature fluctuations depend on the molecular Prandtl number. The strong similarity between $\overline{\theta' v'}$ and $\overline{u' v'}$ has been reported by Perry and Hoffmann (1976), although their measurements were made at $y/\delta = 0.3$ and the similarity between the two was not as strong as the present results.

It appears that one can assume that the behavior of the passive scalar would be the same as that of the streamwise velocity fluctuation in the wall region. It should be interesting to examine whether one can model the fluxes of $\overline{\theta' u'}$ and $\overline{\theta' v'}$ in the same form as models for $\overline{u'^2}$ and $\overline{u' v'}$.

SUMMARY

Direct numerical simulation of a turbulent channel flow with three passive scalars was performed. No turbulence model was used in the computation, since the grid resolution was sufficiently fine to resolve all the essential turbulent scales. Computed statistics were compared with existing experimental data. The mean temperature profiles were in excellent agreements with the formula suggested by Kader (1981). Agreements in other quantities were satisfactory, and the general trend of the turbulent Prandtl number with respect to the molecular Prandtl number was consistent with the existing experimental observations. The computed scalar fields were also examined for structures in the scalar field. It was found that the temperature fields were highly correlated with the streamwise velocity. The streaky structures observed in the wall region were also observed in the temperature field with the same nondimensional mean spacing, almost independent of the molecular Prandtl numbers considered in the present paper. The correlation coefficient between the temperature and the streamwise velocity was as high as 0.95 in the wall region. The joint probability distributions between the temperature and velocity fluctuations and two-point correlations in the wall region suggest that it might be possible to model the scalar fluxes in a manner similar to that used for momentum fluxes.

ACKNOWLEDGMENTS

We are grateful to Drs. S. Lele and M. Rogers for reviewing the manuscript, and to Dr. N. Mansour for helpful discussions during the course of this work.

REFERENCES

Antonia, R. A. (1980), "Behavior of the turbulent Prandtl number near the wall," *Int. J. Heat Mass Transfer* **23**, p906.

Chen, C. H. P. & Blackwelder, R. F. (1978), "Large scale motion in a turbulent boundary layer: a study using temperature contamination," *J. Fluid Mech.* **89**, p1.

Deissler, R. G. (1963), "Turbulent heat transfer and temperature fluctuations on a field with uniform velocity and temperature gradients," *Int. J. Heat Mass Transfer* **6**, p257.

Eckelman, L. D. & Hanratty, T. J. (1972), "Interpretation of measured variations of the eddy conductivity," *Int. J. Heat Mass Transfer* **15**, p2231.

Grotzbach, G., "Numerical simulation of turbulent temperature fluctuations in liquid metals," *Int. J. Heat Mass Transfer* **24**, p475.

Iritani, Y., Kasagi, N. & Hirata, M. (1983), "Heat transfer mechanism and associated turbulence structure in the near-wall region of a turbulent boundary layer," Proceedings of 4th Symposium on Turbulent Shear Flows, Karlsruhe, Germany.

Kader, B. A. (1981), "Temperature and concentration profiles in fully turbulent boundary layers," *Int. J. Heat Mass Transfer* **24**, No. 9, p.1541.

Kim, J., Moin, P. & Moser, R. D. (1987), "Turbulence statistics in fully developed channel flow at low Reynolds number," *J. Fluid Mech.* **177**, p133.

Launder, B. E. (1978), "Heat and Mass Transport," *Turbulence*, edited by P. Bradshaw, Springer-Verlag.

Lumley, J. L. & Khajeh-Nouri, B. (1974), "Computational modeling of turbulent transport," *Adv. Geophys.*, **18A**, p169.

Malhotra, A. & Kang, S. S. (1984), "Turbulent Prandtl number in circular pipes," *Int. J. Heat Mass Transfer* **27**, p2158.

McEligot, D. M., Pickett, P. E. & Taylor, M. F. (1976), "Measurement of wall region turbulent Prandtl numbers in small tubes," *Int. J. Heat Mass Transfer* **19**, p799.

Perry, A. E. and Hoffmann, P. H. (1976), "An experimental study of turbulent convective heat transfer from a flat plate," *J. Fluid Mech.* **77**, p355.

Reynolds, A. J. (1975), "The prediction of turbulent Prandtl and Schmidt numbers," *Int. J. Heat Mass Transfer* **18**, p1055.

Subrmanian, C. S. and Antonia, R. A. (1981), "Effect of Reynolds number on a slightly heated turbulent boundary layer," *Int. J. Heat Mass Transfer* **24**, No. 11, p1833.

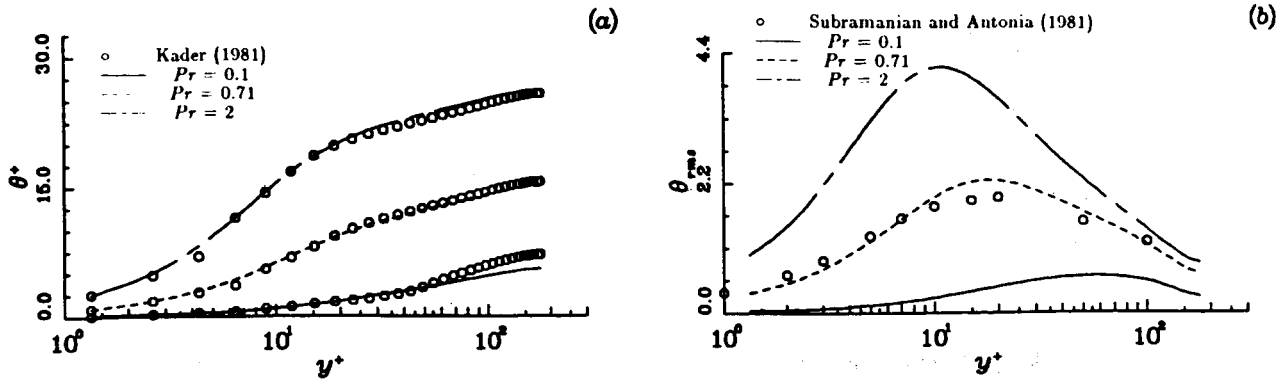

Fig. 1 Profiles of a) mean and b) *rms* fluctuations of the scalar fields.

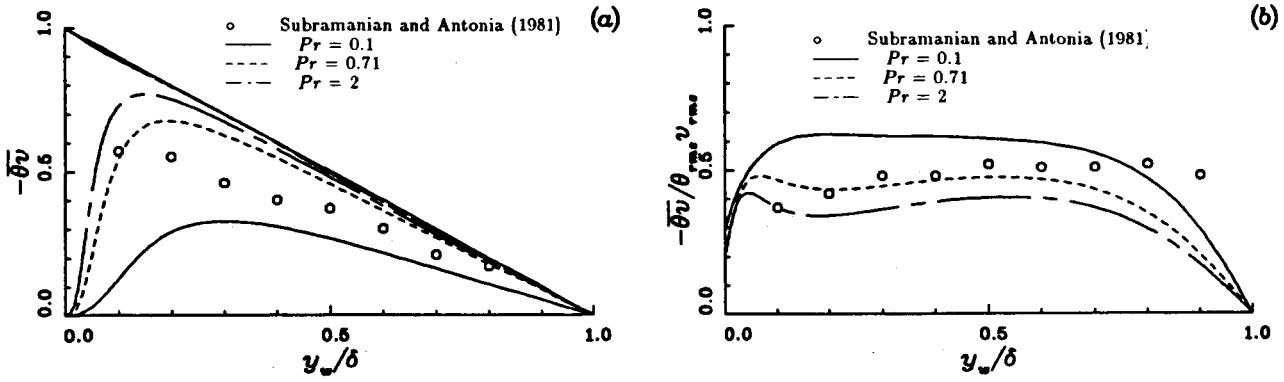

Fig. 2 Profiles of a) the normal heat flux, $-\overline{\theta' v'}$ and b) its correlation coefficient.

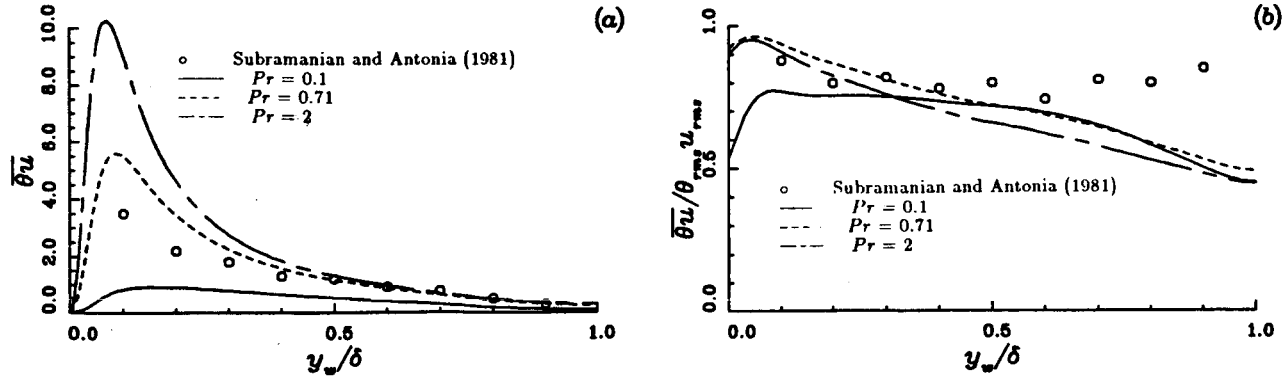

Fig. 3 Profiles of a) the axial heat flux, $-\overline{\theta' u'}$ and b) its correlation coefficient.

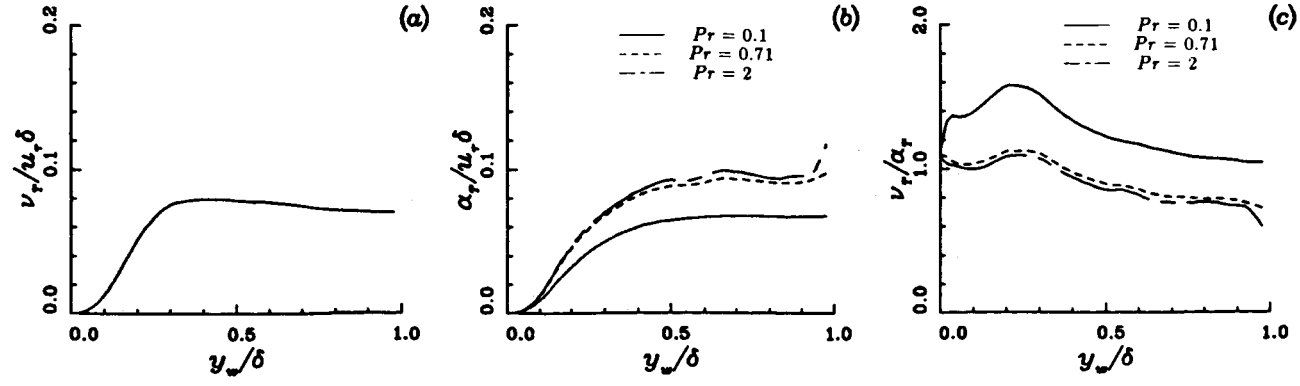

Fig. 4 Profiles of a) eddy viscosity, b) eddy diffusivity and c) turbulent Prandtl number.

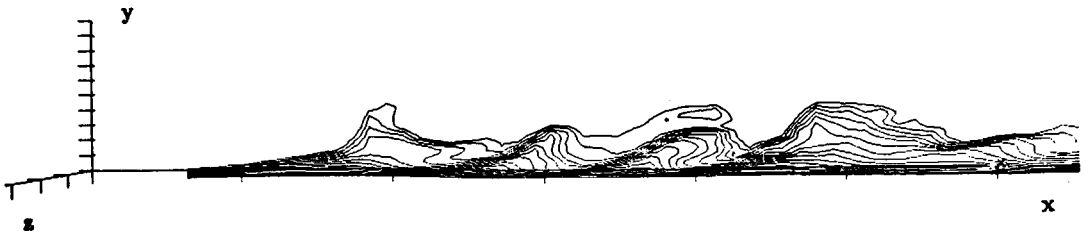

Fig. 5 Contours of a temperature field in an (x, y)-plane; mean flow direction is from left to right.

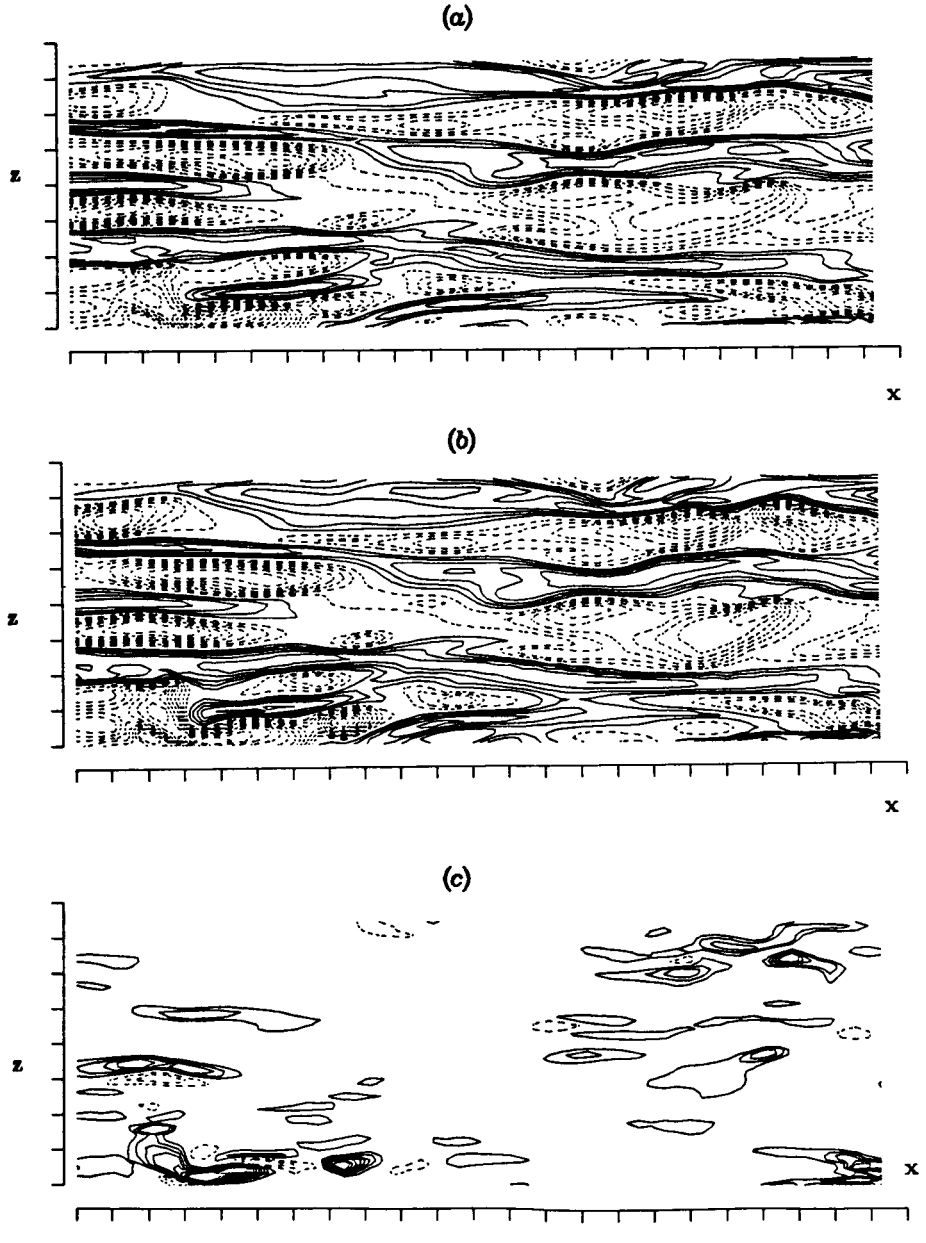

Fig. 6 Contours of a) streamwise velocity fluctuations, b) temperature, and c) $\overline{\theta' v'}$ in the (x, z)-plane at $y^+ \approx 5$. The solid lines represent negative quantities and the dashed lines represent positive quantities. The field shown here is a small portion of the computational domain, and the tick marks denote $50\ \nu/u_\tau$.

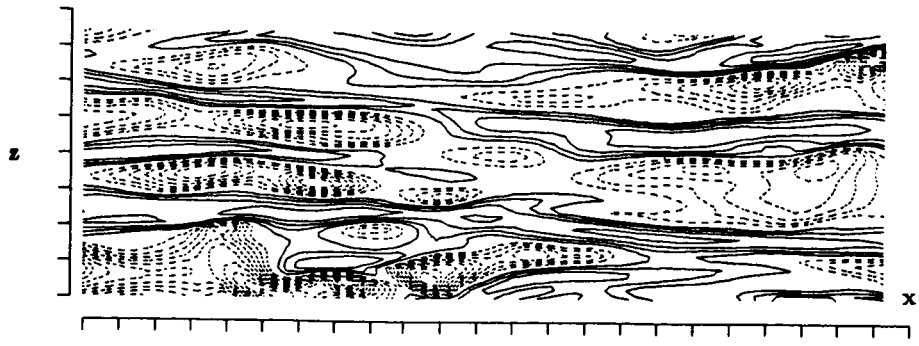

Fig. 7 Contours of the surface heat flux fluctuations. See Fig. 6 captions for legends.

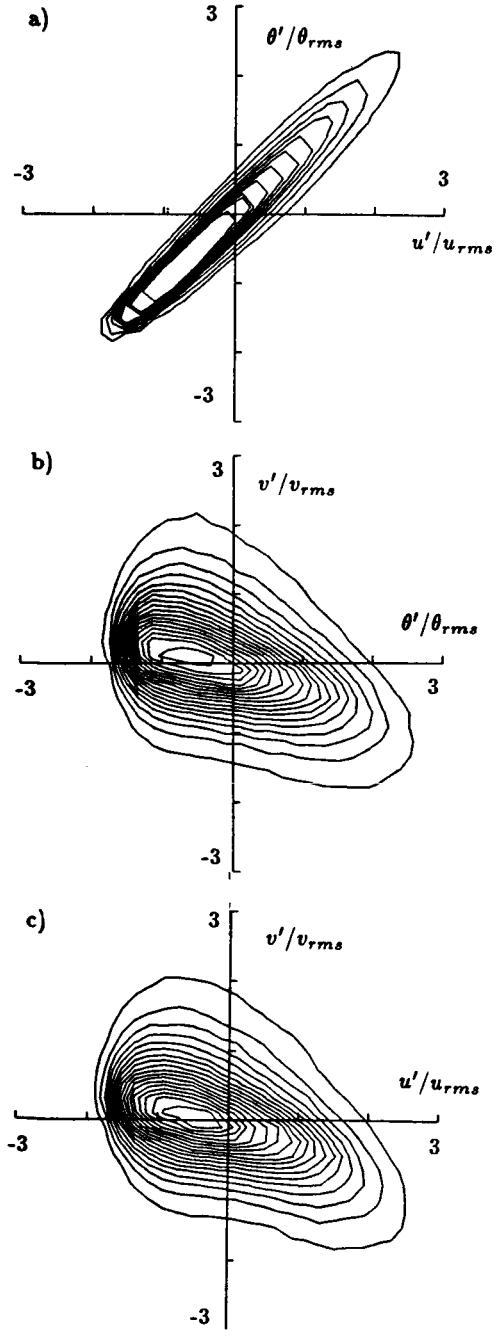

Fig. 8 The joint probability distributions of a) u', θ', b) θ', v', and c) u', v' at $y^+ \approx 5$ for Pr=0.71.

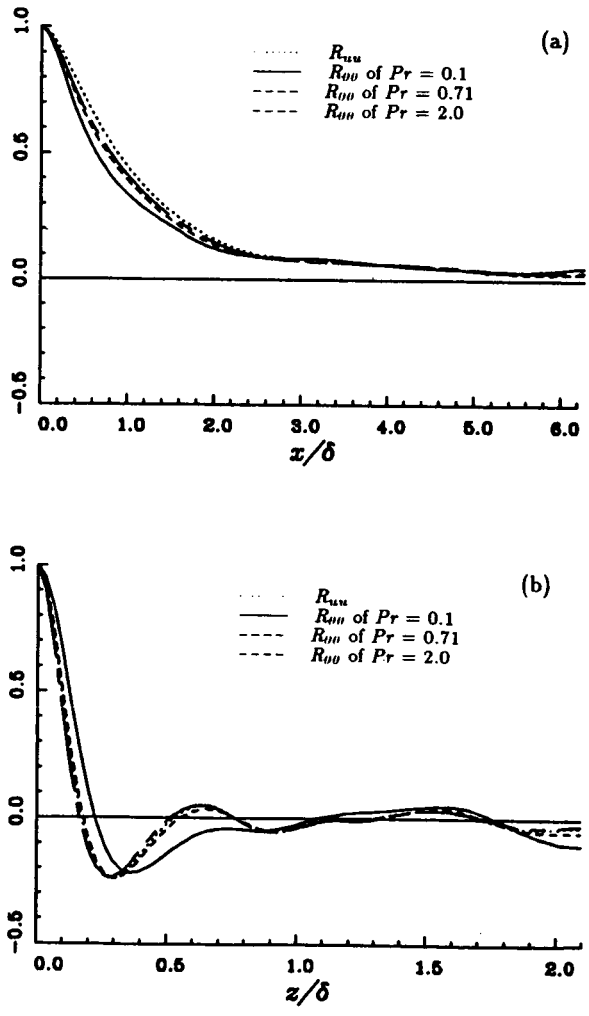

Fig. 9 Two-point correlations of streamwise velocity and temperature fluctuations at $y^+ \approx = 5$: a) streamwise separation; b) spanwise separation. $x/\delta = 1$ corresponds to $xu_\tau/\nu \approx 180$.

NASA National Aeronautics and Space Administration

Report Documentation Page

1. Report No.	2. Government Accession No.	3. Recipient's Catalog No.
NASA TM-89463		

4. Title and Subtitle	5. Report Date
Transport of Passive Scalars in a Turbulent Channel Flow	July 1987
	6. Performing Organization Code

7. Author(s)	8. Performing Organization Report No.
John Kim and Parviz Moin	A-87235
	10. Work Unit No.

9. Performing Organization Name and Address	11. Contract or Grant No.
Ames Research Center Moffett Field, CA 94035	
	13. Type of Report and Period Covered
12. Sponsoring Agency Name and Address	Technical Memorandum
National Aeronautics and Space Administration Washington, D.C. 20546	14. Sponsoring Agency Code 505-31-01

15. Supplementary Notes

Point of contact: John Kim, Ames Research Center, MS 202A-1, Moffett Field, CA 94035 (415)694-5867 or FTS 464-5867.

16. Abstract

A direct numerical simulation of a turbulent channel flow with three passive scalars at different molecular Prandtl numbers is performed. Computed statistics including the turbulent Prandtl numbers are compared with existing experimental data. The computed fields are also examined to investigate the spatial structure of the scalar fields. The scalar fields are highly correlated with the streamwise velocity; the correlation coefficient between the temperature and the streamwise velocity is as high as 0.95 in the wall region. The joint probability distributions between the temperature and velocity fluctuations are also examined; they suggest that it might be possible to model the scalar fluxes in the wall region in a manner similar to the Reynolds stresses.

17. Key Words (Suggested by Author(s))	18. Distribution Statement
Turbulence Passive scalars Numerical simulation	Unlimited - Unclassified Subject category: 34

19. Security Classif. (of this report)	20. Security Classif. (of this page)	21. No. of pages	22. Price
Unclassified	Unclassified	12	A02